Original Scientific Article • DOI: 10.2478/rmzmag-2023-0002

Received: January 01, 2023
Accepted: February 20, 2023

Geology and Rare Earth Element Geochemistry of Magnesian Granitoids Within Proterozoic Schist Belt of Southwest Nigeria

Geologija in geokemija redkih zemelj iz magnezijevih granitoidov proterozojskega pasu skrilavca v JZ Nigeriji

Olufemi Williams Okunola[1], Akinade Shadrach Olatunji[2], Adegoke Olukayode Afolabi[3,*]

[1]Nigerian Geological Survey Agency, P.M.B. 616, Utako District, Abuja, Nigeria

[2]Department of Geology, University of Ibadan, Ibadan, Nigeria

[3]Department of Earth Science, Ladoke Akintola University of Technology, Ogbomoso, Nigeria

*Corresponding author: E-mail: oaafolabi@lautech.edu.ng

Abstract

The increased global demand for and price of rare earth elements (REEs) has led to intensive search for them in rocks of the upper continental crust all over the world. This study is aimed at characterising the granitoids at Okeho within Southwestern Nigeria using geochemical data and assessing their potential for REE enrichment. Ten representative rock samples of the Proterozoic intrusives, syenite and granodiorite, were studied for their mineralogical and elemental compositions. Elemental concentrations were analysed using Inductively Coupled Plasma Mass Spectrometry (ICP-MS).

Average major oxide concentrations revealed SiO_2 (57.53 wt. %), Al_2O_3 (13.25 wt. %), CaO (5.05 wt. %), and MgO (5.59 wt. %) for the syenite and SiO_2 (62.39 wt. %), Al_2O_3 (14.98 wt. %), CaO (3.67 wt. %), and MgO (3.25 wt. %) for the granodiorite. Total Alkali–Silica (TAS), Aluminum Saturation Index (ASI), and La/10-Y/15-Nb/8 plots discriminated the granitoids as metaluminous monzonite-syenite and peraluminous diorite-granodiorite. Average total REE concentrations in the syenite (625.06 ppm) and porphyritic-granodiorite (364.51 ppm) were above values reported for the granites in some mines in Jiangxi Province, Southern China.

Keywords: major oxides, REE, syenite, granodiorite, orogenic-setting

Povzetek

Porast globalnih potreb po redkih zemljah (REE) in dvig njihovih cen sta povzročila intenzivno iskanje ustreznih rudnin v zgornjem delu zemeljske skorje po celem svetu. Namen pričujoče raziskave je karakterizacija granitoidnih kamnin v okolici Okeha v jugozahodni Nigeriji ter na podlagi geokemičnih podatkov podati njihov potencial za REE. Določili smo mineraloško in elementarno sestavo desetih reprezentativnih vzorcev proterozojskih intruzij, sienita in granodiorita. Koncentracije elementov so bile določene z masno spektrometrijo z induktivno sklopljeno plazmo (ICP-MS).

Glavni oksidi in njihove povprečne koncentracije v sienitu so SiO_2 (57,53 ut. %), Al_2O_3 (13,25 ut. %), CaO (5,05 ut. %) in MgO (5,59 ut. %), v granodioritu pa SiO_2 (62,39 ut. %), Al_2O_3 (14,98 ut. %), CaO (3,67 ut. %), in MgO (3,25 ut. %). Skupna vsebnost alkalij proti kremenici (TAS), indeks nasičenosti z aluminijem (ASI) in diagrami La/10-Y/15-Nb/8 ločujejo granitoide na metaluminozni monzonit-sienit in peraluminozni diorit-granodiorit. Povprečne vsebnosti REE v sienitu (625,06 ppm) in porfiritnem granodioritu (364,51 ppm) so višje od vrednosti v granitih nekaterih rudnikov Jiangxi province v južni Kitajski.

Ključne besede: glavni oksidi, REE, sienit, granodiorit, območje orogena

Introduction

The global demand for oxides of rare earth elements (REEs) has increased tremendously, and it is believed that the world may soon face a shortage of REEs. China is the leading global producer of REEs and tends toward a monopolistic market that can force hikes in the prices of REEs [1]. Concern regarding that tendency is no longer speculation, as China, the world leading producer of REE in 2010, is making significant export cuts and restrictions. The increased demand for and rising prices of REEs have necessitated intensive searches for these metals globally. These elements have been sourced mostly from carbonatite, ion-adsorbed clays, weathered crusts of granites, deposits hosted by metamorphic rocks, placer deposits and paleo-placers, alkaline igneous complexes, phosphorites, uranium deposits, igneous affiliated deposits, bauxite, and laterite hosted deposits [2–5] and have found immense use in renewable energy and technology.

In 2009, the British Geological Survey and Nigerian Geological Survey Agency carried out a regional geochemical survey of Southwestern Nigeria using stream sediments. Their report identified anomalous concentrations of REEs. Based on their report, the Ikomu area, Sheet 220, was selected for further work on REE mineral potential within Southwestern Nigeria. This work investigated the granitoids of the area for REE occurrences, abundances, and prospects since it falls into one of the sources of REE as documented in Orris and Grauch [2]. Few documented works on the assessment of REE in the granitoids of Southwestern Nigeria exist. Some of these reports have suggested that most felsic rocks of the Precambrian basement complex of Southwestern Nigeria showed considerable evidence for crustal assimilation, which has enhanced light rare earth elements (LREE) enrichment in particular [6–8]. REE abundances in the crust have shown that, though relatively low in abundance, some have crustal concentrations relatively higher than some precious metals. For example, Ce and Y have concentrations higher than Sn, Hg, Mo, and all precious metals [9]. Crustal abundances of elements are largely derived from felsic rocks that dominate the upper continental crust, hence the exploration for REEs in granite.

Granite geochemistry is varied, and this is largely due to the nature of its origin. Granitoids chemically reflect their source, and their source serves as the basis for granite classification [10, 11]. However, the chemical compositions, especially trace elements, are varied and may be responsible for difficulties when attempting a generalised geochemical characterisation. This may be linked with possible hybrid sources of granites. Partial melting and assimilation processes are dominant activities that cause hybridisation of granites.

Granite occurrences characterise several tectonic settings such as plate boundaries and intra-plates. Granites from these settings have been designated either as (i) oceanic ridge granites (ORG); (ii) within plate granites (WPG); (iii) volcanic arc granite (VAG); and (iv) collision granite (COLG) [12]. The COLG was further divided into (1) pre-collision; (2) syn-collision, and (3) post-collision [13]. Plate tectonic processes that form subduction-related orogens characterised by (1) an accretionary complex associated closely with high temperature/pressure metamorphic belt; (2) a fore-arc basin deposit; and (3) a magmatic province within a high temperature/pressure metamorphic belt at continental margins are called 'cordilleran-type' orogeny [14]. The cordilleran orogeny that spanned from Late Triassic to Early Tertiary has been studied in depth. Granites from this orogen are rich in gold and REEs [15]. This study is aimed at undertaking a geochemical assessment of major oxides and REE in granitoids that are part of Ikomu, Sheet 220, Southwestern Nigeria, in order to use geochemistry to characterise and evaluate them as possible sources of REEs.

Geological setting of study area

Lithological relationship

Granitoid occurrences in the basement complex of Southwestern Nigeria are distinguished as Older granites. The Older granites are Precambrian in age, in contrast to the Mesozoic Younger granites localised in the north-central part of Nigeria. These granitoids occur mostly as intrusions into schistose rocks which

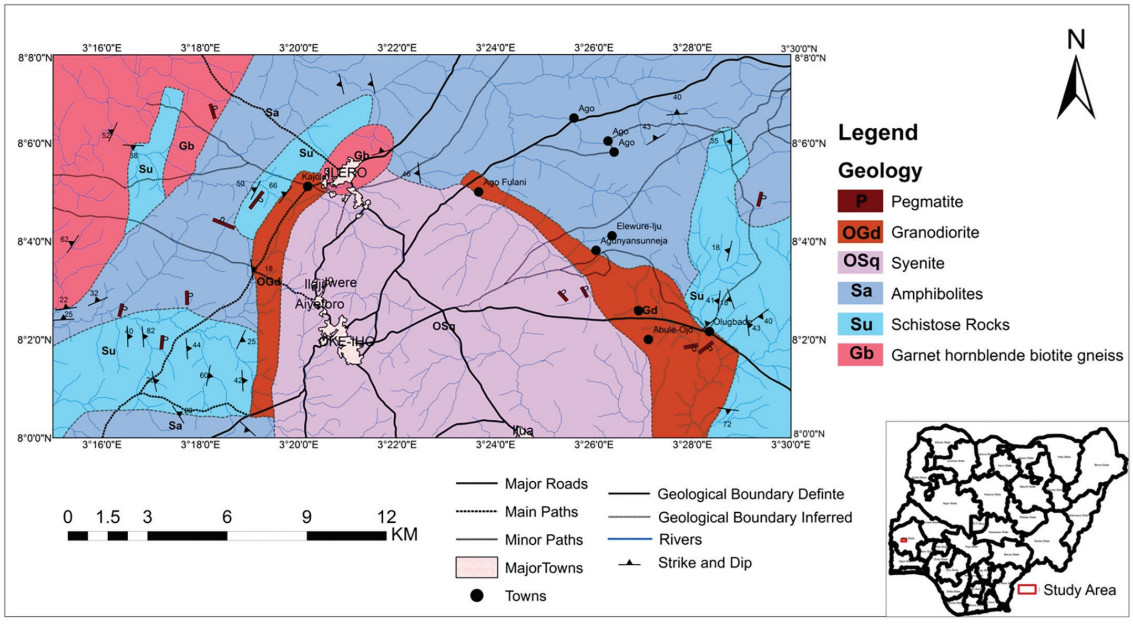


Figure 1: *Geological map of the study area.*

overlie migmatitic gneisses. Most schistose rocks occur as narrow belts that are infolded into older Precambrian rocks which are predominantly gneissose in structure. The granitoids and the schistose rocks host pegmatitic veins that are mineralised in gold, tantalite-columbite, and gemstones such as tourmaline and aquamarine. These areas have also been sites for mining feldspars and muscovite in commercial quantities. Granitoid bodies, in Southwestern Nigeria, outcrop dominantly as alkali granites, quartz monzonites/diorites/granodiorites, syenites, and tonalities. Syenite bodies in Southwestern Nigeria have been described from Igboho, Shaki, Okeho and Iwo [16, 17]. These exposures are rich in potassic feldspars and pyroxenes. Within Southwestern Nigeria, the granodiorites and the alkali granites are more widespread than the syenites. The Okeho area within the Oyan-Iseyin Schist Belt is predominantly underlain by rocks of the Proterozoic era. Within the Okeho area, both syenite and granodiorite bodies occur in close association with biotite and talc schist to the south, pelitic schist to the northeast, and amphibolite to the north (Figure 1). These rock units are underlain by the migmatitic gneiss which is observed to outcrop in the northwestern area.

The migmatitic gneiss and the amphibolite are the oldest rock units in the area and were observed as low-lying units. The migmatitic gneiss has a simple mineralogy consisting of quartz, feldspar, and biotite with accessory amounts of garnet. The garnet crystals were observed as euhedral grains that are dark red in colour, suggestive of almandine garnet. Elueze [18] described four petrographically distinct amphibolite rocks within the southwest of Nigeria. In this study, two amphibolite rock types were identified as the foliated and massive types. The dominant mineralogy consists of hornblende and plagioclase. The massive amphibolite, where exposed, often host quartz veins which occasionally formed into large grains.

Lithological associations revealed granitoid intrusives into the garnet-biotite–rich gneiss overlain by schistose rocks of varied mineralogical composition from garnet-rich pelitic schist, biotite-rich schist to talc schist. This granitoid pluton is elliptical in outline and hilly in exposure. The granitoids display porphyritic texture at the northern margins where it shares boundary with amphibolite and the pelitic schist exposures. While at the core of the pluton, the granitoid is characteristically graded into different shades of grey to pinkish colour

in appearance. Hand specimen samples suggest that the colour variation may be attributed to the varied modal proportions of feldspar and pyroxene compositions.

Petrological evidence contrasted the core of the granitoid into a quartz-saturated syenite at the core and a granodiorite part restricted to some areas in the northern margins of the granitoid. The granodiorite shares boundaries with the pelitic schist and the amphibolite. Field evidence at one of the boundary sites revealed inclusions of schist and amphibolitic xenolith pods within the granitoid body. Field evidence revealed textures from granular to porphyritic at the boundaries shared with the granodiorite, suggesting a gradational boundary. Amphibolite inclusions are common in the syenite core. These inclusions occur as elongated spindle-like bodies with their longer axes aligned parallel to the direction of alignment of the microcline phenocrysts.

Both the syenite and the granodiorite bodies are characterised by coarse grains of feldspars having distinctive twinning according to the pericline law. Within the syenite, the fabric is granular, while it is porphyritic in the enveloping granodiorite. Quartz grains are common and large in hand specimen samples of the granodiorite but sparse and smaller in dimension in the syenite.

Materials and methods

Lithological field mapping of the study area was carried out on a scale of 1:20,000 to establish the rock types and their distribution. Sixty representative rock samples were collected. From these, twenty-two representative hand specimen samples (twelve from the syenite and ten from the granodiorite) were selected and studied for textural and mineral identification purposes. For the petrographic studies, the rock samples were cut to 0.3 mm thickness and mounted onto 1 in x 3 in slides, and the slides were studied using a petrological microscope for mineral identification and description at the Department of Earth Science, Ladoke Akintola University of Technology, Ogbomoso. Physical counts were used to determine the modal mineralogy.

From the 22 rock samples used for the petrographic study, 10 samples (7 syenite rock samples and 3 granodiorite samples) were selected for chemical analysis to determine elemental concentrations. These rock samples were pulverised and sieved to <63 μm. Portions of the <63 μm fractions of sieved samples were digested using aqua regia. To achieve total digestion, 0.5 g each of the pulverised samples (<63 μm) were dissolved in hot acids of HF, HCl, HNO_3, and $HClO_4$ in the ratio of 1:1:1:1. The digested samples were analysed for major oxides and REE compositions using the Inductively Coupled Plasma Mass Spectrometer (ICP-MS) in Acme Analytical Laboratories Ltd., Vancouver, Canada.

Results and discussion

Mineralogy and petrography

Granodiorite: Minerals identified from hand specimen samples of the granodiorite include quartz, biotite, and twinned alkali feldspar, according to the Pericline law. Thin section analysis revealed quartz, biotite, microcline, plagioclase, and muscovite (Figure 2). The abundance of felsic minerals defined a low colour index, hence the rock is described as leucocratic. Modal composition shows that the granodiorite is rich in quartz and biotite (Table 1). Thin sections revealed two types of twinning in the feldspars, one according to Albite Law and the other is Crosshatch (tartan) twinning. Based on this respective twinning both albite and microcline feldspars were identified. Grain sizes of plagioclase ranged from medium (0.6 cm x 0.7 cm to 1.2 cm x 3.4 cm) to coarse (3.6 cm x 2.4 cm to 1.8 cm x 5.9 cm). The alkali feldspar grains in the granodiorite are coarse and elongated with the longer axis reaching 6 cm–10 cm in many grains and are uniformly pinkish in colour. Biotite and hornblende grains constitute the other major minerals while apatite and zircon grains occurring in accessory amounts were observed as inclusions in plagioclase and biotite grains, respectively. The presence of normative corundum (C) and rutile (R), and the absence of diopside (Di) and sphene (Tn) contrast the granodiorite from the syenite (Table 2).

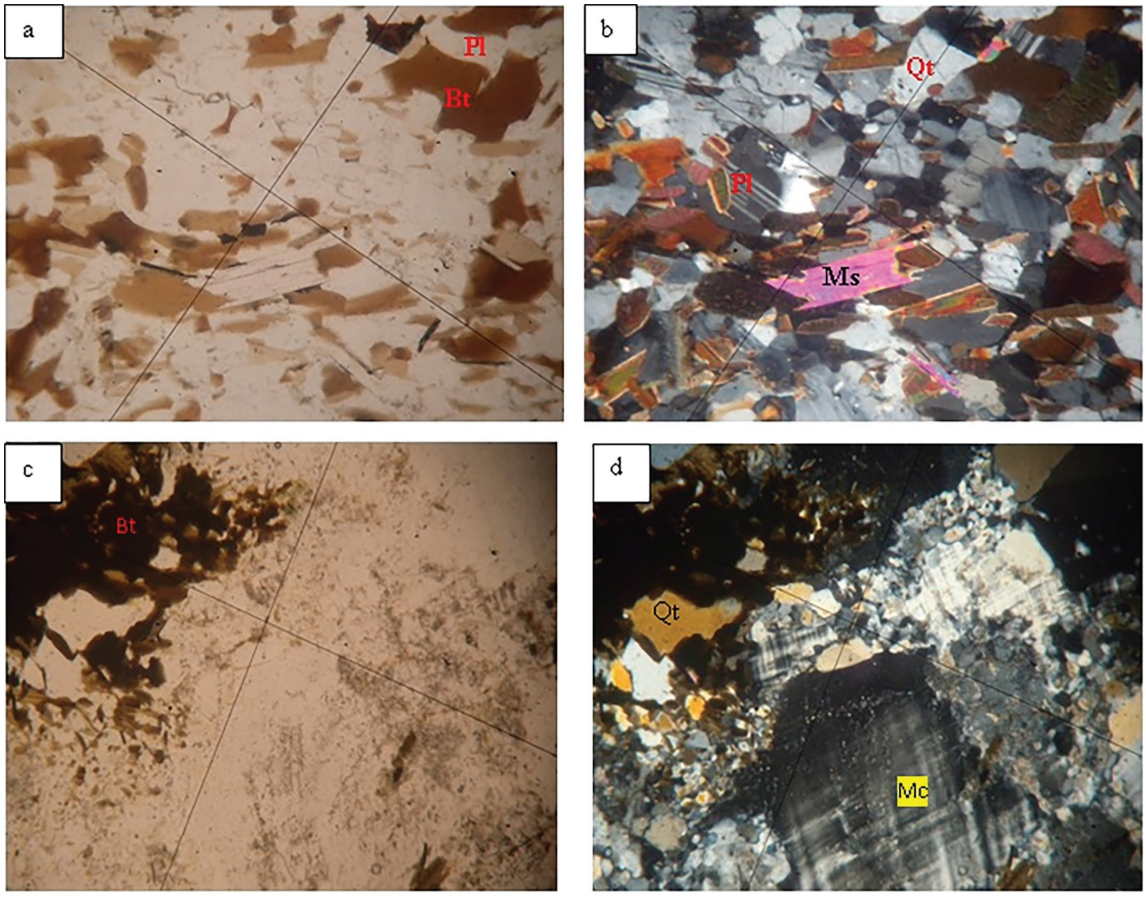


Figure 2: *a) Plane polar photomicrograph of the granodiorite reveals biotite (Bt) as the main mineral phase. b) Plagioclase (Pl), muscovite (Ms), and quartz (Qz) are identified as other major mineral phases under cross-polar. c) Biotite crystals forming mantle around large phenocrysts of feldspar are identified in plane polar. d) Porphyroclast of microcline shows evidence for grain size reduction in cross-polar. The magnification of photomicrographs is x40.*

Table 1: *Modal mineralogy for the studied granitoids.*

Min/Sample Id	Pg1	Pg2	Pg3	Sy1	Sy2	Sy3	Sy4	Sy5	Sy6	Sy7
Quartz	44	46	47	4	2	4	8	10	7	8
Microcline	13	7	12	42	43	42	41	44	45	42
Plagioclase	12	13	11	20	30	16	15	20	20	20
Hornblende	7	6	5	15	13	17	16	14	13	15
Pyroxene	–	–	–	3	2	5	6	6	5	4
Biotite	21	23	20	15	9	15	12	5	8	9
Opaque	3	5	5	1	1	1	2	1	2	2
Garnet	–	–	–	1	1	1	3	2	2	3

Syenite: The feldspar grains in the syenite occur as rectangular equant laths ranging in length of the long axis from 1 cm to approximately 6 cm. Other minerals visible in hand specimens are plagioclase, pyroxene, and biotite. The modal mineralogy as presented in Table 1 from thin section analysis reveals phenocrysts of sanidine, plagioclase, quartz, hornblende, pyroxene, garnet, and minor amounts of biotite, while in the fine groundmass quartz, biotite, and pyroxene were identified together with accessory amounts of opaque minerals

Table 2: *Cross, Iddings, Pirsson, and Washington (CIPW) normative mineralogy normative mineralogy for the studied granitoids.*

Norm	Pg1	Pg2	Pg3	Sy1	Sy2	Sy3	Sy4	Sy5	Sy6	Sy7
Q	28.634	23.272	17.188	5.931	7.31	2.392	5.254	7.09	5.593	5.531
C	3.16	2.875	0	0	0	0	0	0	0	0
Or	19.798	19.088	34.513	30.967	41.073	38.413	35.99	39.891	40.718	39.95
Ab	17.008	22	15.4	8.462	23.354	24.201	15.823	21.154	19.293	18.193
An	11.78	14.029	14.774	9.258	7.74	5.428	7.644	6.414	7.152	6.81
Di	0	0	0	18.297	3.849	10.891	13.522	9.775	9.623	11.402
Hy	9.142	8.37	8.096	13.763	6.163	6.335	9.102	4.487	5.728	6.572
Il	0.235	0.193	0.15	0.257	0.193	0.193	0.278	0.193	0.171	0.214
Hm	7.381	6.411	5.65	7.481	5.94	6.451	7.801	6.07	6.08	6.301
Tn	0	0	0.993	2.786	2.108	2.844	1.776	2.255	2.627	2.399
Ru	1.007	0.879	0.457	0	0	0	0	0	0	0
Ap	0.64	1.587	0.734	1.113	0.9	1.137	1.042	0.829	1.161	1.184
Sum	98.784	98.704	97.955	98.315	98.629	98.284	98.233	98.158	98.145	98.556

(Figure 3). Field evidences revealed colour variations, from pink to dark grey, for the alkali feldspars within the syenite core. Thin section analysis revealed the presence of pyroxene in the syenite and its absence in the granodiorite. The syenite containing pyroxene and modal quartz is interpreted as quartz-saturated syenite. Modal composition (Table 1) reveals an abundance of hornblende and microcline over the adjoining granodiorite. Normative mineralogy (Table 2) showed that the syenite is richer in hypersthene (Hy) and lower in quartz (Q).

Geochemical Characterisation and Petrogenesis

The granitoids of Okeho do not show a wide range of silica concentration (55.04–63.70 wt. %) as presented in Table 3a, despite their petrological contrast. SiO_2 values ranged from 55.04–59.77 wt. % for the syenite and 61.65–63.70 wt. % for the granodiorite. The respective average MgO and CaO values observed were 3.43 wt. % and 3.37 wt. % for the granodiorite and 5.05 wt. % and 5.59 wt. % for the syenite. K_2O values were observed to be higher than Na_2O values in both rock types (Table 3). In Figure 4, the sample plots of SiO_2 vs. Na_2O and K_2O suggest slightly varied mineral fractionation with the granodiorite being less enriched in alkali-rich mineral phases. This is also consistent with the observed modal and normative mineralogy (Tables 1 and 2).

SiO_2 and Na_2O+K_2O concentrations, from major oxides presented in Table 3a, when plotted in the TAS plot by Middlemost [19] (Figure 5), characterised samples from the syenite pluton as dominantly monzonitic and samples from the granodiorite as granodioritic/dioritic to quartz-monzonitic. From the Cross, Iddings, Pirsson, and Washington (CIPW) normative mineralogy, an adapted QAP diagram [20] showed that the syenite samples are quartz-syenitic to quartz-monzonitic in character while the samples from the granodiorite are granodioritic (Figure 6). Granite lineages [21, 22] on the Streckeisen triangle were distinguished by Bowden [23] as CAT – calcalkaline tonalitic or trondhjemitic, CAG – calcalkaline granodiorite, SAM – subalkaline monzonitic, ALK – aluminous potassic, and ANA – alkaline soda. The characters of the syenite and granodiorite rock samples of the study are consistent with some of the generalised fields of granite lineages. The syenites share the subalkaline monzogranite (SAM) nature while the granodiorites share that of the calc-alkaline granodiorites (CAG).

Figure 7a is a plot of SiO_2 vs. $FeO_{(tot)}/MgO$ [24] illustrating all granitoid samples plotted in the calc-alkaline field, and the adapted plot

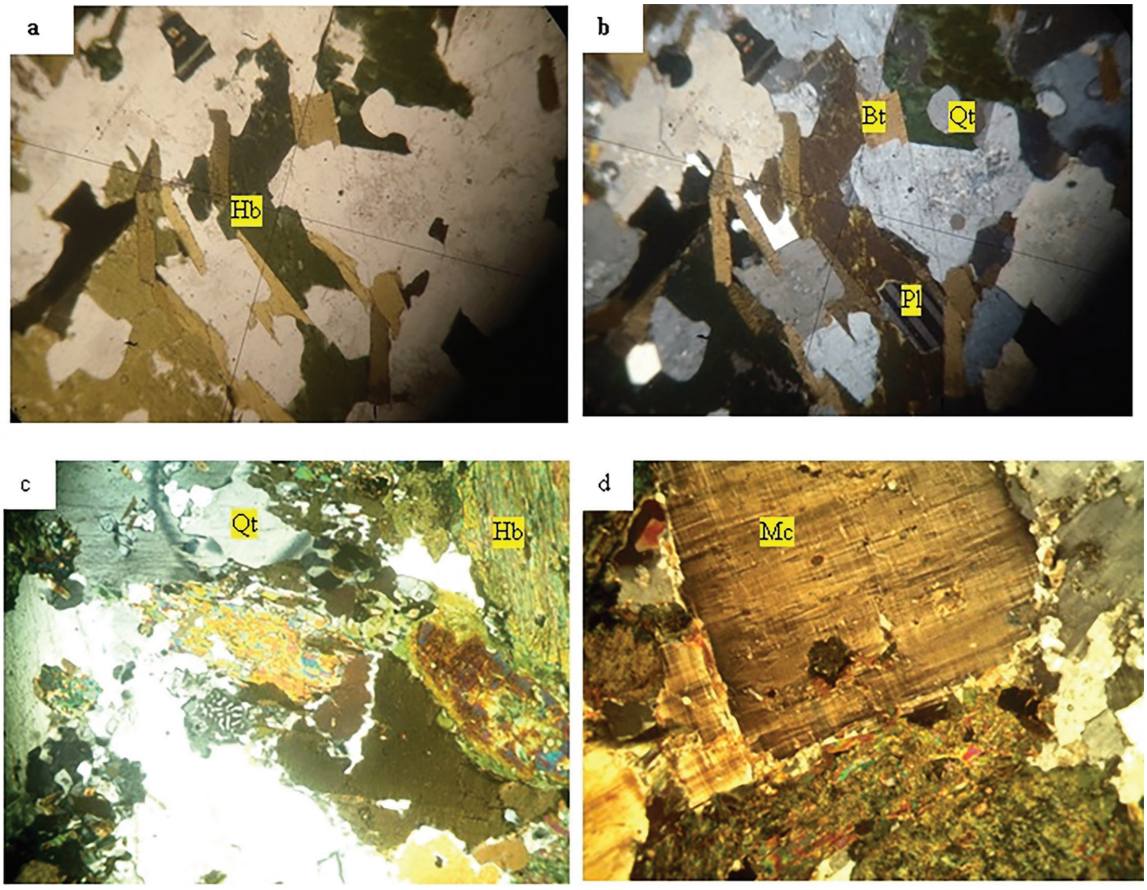


Figure 3: *Photomicrograph of syenite. a) Plane-polarised light reveals euhedral grains of biotite (Bt) around subhedral grains of hornblende (Hb). b) Cross-polar view reveals plagioclase (Pl) and quartz (Qt) as the main mineral phases. c) and d) reveal large hornblende and microcline grains. The magnification of photomicrographs is x40.*

of Al_2O_3/SiO_2 vs. MgO/SiO_2 [25] (Figure 7b) suggests that the calc-alkaline primary magma is derived, probably, from partial melting of either mantle-derived mafic underplate or lower crust with crust contribution [26]. At low pressures, partial melting of tonalitic to granodioritic crust yields alkali-calcic to calc-alkalic granitoids that are metaluminous while peraluminous rocks are produced at high pressures [27]. These granitoids are magnesian (Figure 8a) with calc-alkali, alkali-calcic to alkalic characters (Figure 8b).

From Figure 8c, the plot of SiO_2 vs. K_2O, the primitive magma that possibly formed the granitoids of the study typifies the High-K calc-alkaline–Shoshonitic magma series. This character is consistent with the K-feldspar porphyritic texture granodiorite (KCG) type described by Barbarin [26]. High-K calc-alkaline granitoids are typical products of subduction zone processes [26, 28, 29].

The Aluminium Saturation Index (ASI) [32] is the molecular ratio Al/(Ca – 1.67P + Na + K) and accounts for excess Al that can be accommodated within feldspar crystal lattices and therefore accounts for the formation of other mineral phases, such as aluminous biotite in weakly peraluminous or muscovite, cordierite, garnet, or kyanite/andalusite/sillimanite (Al_2SiO_5 polymorphs) in strongly peraluminous rocks. The ASI for peraluminous rocks is greater than 1. When ASI < 1 and molecular Na+K < Al the rock has a metaluminous character, where Al is used up in the formation of feldspars and excess Ca is used in the formation of calcic mineral phases such as augite and hornblende. If ASI < 1 and Na+K > Al the rock is peralkaline and hornblende is formed in weakly peralkaline or sodic amphiboles and pyroxenes are formed in strongly peralkaline [11]. The ASI value for each of the syenites is less than 1 (Table 3) and illustrated in the plot of A/CNK

Table 3: *Elemental concentrations of the studied granitoids. Granodiorite (Pg1–Pg3) and Syenite (Sy1–Sy7) (major oxides are in wt. % and trace element in ppm).*

Sample id	Pg1	Pg2	Pg3	Av.	Sy1	Sy2	Sy3	Sy4	Sy5	Sy6	Sy7	Av.	Ave*
SiO_2	63.70	61.82	61.65	62.39	55.04	59.77	56.95	56.23	59.03	57.88	57.84	57.53	58.99
Al_2O_3	14.41	15.79	14.73	14.98	10.71	14.90	13.73	12.47	13.77	13.83	13.35	13.25	13.77
Fe_2O_3	7.38	6.41	5.65	6.48	7.48	5.94	6.45	7.80	6.07	6.08	6.30	6.59	6.56
MgO	3.67	3.36	3.25	3.43	8.93	3.19	4.57	6.17	3.62	4.09	4.76	5.05	4.56
CaO	2.73	3.71	3.67	3.37	8.02	3.66	5.36	6.13	4.93	5.33	5.67	5.59	4.92
Na_2O	2.01	2.60	1.82	2.14	1.00	2.76	2.86	1.87	2.50	2.28	2.15	2.20	2.19
K_2O	3.35	3.23	5.84	4.14	5.24	6.95	6.50	6.09	6.75	6.89	6.76	6.45	5.76
TiO_2	1.13	0.98	0.94	1.02	1.27	0.96	1.26	0.87	1.02	1.16	1.09	1.09	1.07
P_2O_5	0.27	0.67	0.31	0.42	0.47	0.38	0.48	0.44	0.35	0.49	0.50	0.44	0.44
MnO	0.11	0.09	0.07	0.09	0.12	0.09	0.09	0.13	0.09	0.08	0.10	0.10	0.10
Ba	677.00	685.00	1629.00	997.00	1407.00	1313.00	1387.00	1370.00	1288.00	1402.00	1638.00	1400.71	1279.60
Ni	60.10	57.80	51.90	56.60	114.50	33.10	38.70	26.20	17.40	44.90	44.50	45.61	48.91
Co	22.00	18.90	18.90	19.93	34.10	16.20	22.10	23.30	18.70	19.50	21.30	22.17	21.50
Nb	20.50	16.60	21.60	19.57	21.10	38.90	55.80	22.10	50.20	39.10	31.40	36.94	31.73
Rb	150.50	144.00	250.70	181.73	221.40	341.90	324.70	247.00	388.00	351.70	329.00	314.81	274.89
Sn	3.00	3.00	4.00	3.33	6.00	9.00	11.00	5.00	5.00	6.00	6.00	6.86	5.80
Sc	13.00	12.00	13.00	12.67	21.00	11.00	11.00	16.00	11.00	9.00	13.00	13.14	13.00
Sr	219.00	293.80	387.00	299.93	338.10	449.90	461.80	403.10	402.20	450.70	472.40	425.46	387.80
Ta	1.20	1.20	1.00	1.13	0.90	1.70	2.50	1.50	3.30	2.40	1.80	2.01	1.75
Th	17.20	38.80	26.00	27.33	25.20	48.80	92.90	46.30	53.80	50.20	80.90	56.87	48.01
U	4.10	5.80	5.80	5.23	7.90	5.30	5.20	4.70	6.20	6.70	7.90	6.27	5.96
V	139.00	79.00	82.00	100.00	122.00	73.00	93.00	105.00	87.00	79.00	93.00	93.14	95.20
W	1.40	0.80	0.70	0.97	0.90	1.80	1.50	4.40	1.50	1.70	1.50	1.90	1.62
Hf	15.80	15.00	11.30	14.03	15.30	18.40	17.80	9.30	19.70	15.10	14.30	15.70	15.20
Zr	612.20	605.30	431.70	549.73	625.70	694.10	681.60	324.10	731.60	579.30	559.00	599.34	584.46
Y	69.40	67.40	22.50	53.10	29.00	33.70	47.60	37.60	59.70	34.70	36.50	39.83	43.81
Cu	16.40	13.90	46.50	25.60	104.10	34.80	45.70	23.70	6.60	35.30	37.30	41.07	36.43

(*Continued*)

Table 3. *Continued*

Sample id	Pg1	Pg2	Pg3	Av.	Sy1	Sy2	Sy3	Sy4	Sy5	Sy6	Sy7	Av.	Ave*
Pb	3.90	5.40	12.60	7.30	11.20	34.30	62.50	16.30	10.40	4.80	6.30	20.83	16.77
Zn	104.00	95.00	73.00	90.67	25.00	57.00	35.00	22.00	34.00	55.00	49.00	39.57	54.90
Au	2.10	1.90	0.60	1.53	2.30	0.80	3.20	1.80	0.80	13.90	1.70	3.50	2.91
La	57.8	101.3	76.3	78.47	45.5	149.9	183.5	106.2	248.7	151.2	123.4	144.06	124.38
Ce	99.1	200.9	146.3	148.77	105.6	295.6	350.4	221	421.1	282.4	247	274.73	236.94
Pr	12.86	24.44	17	18.10	14.33	32.95	40.53	26.73	51.53	32.92	29.02	32.57	28.23
Nd	50.3	93.3	61.6	68.40	63.3	115.9	150.6	102.1	181.5	116.9	105.4	119.39	104.09
Sm	9.96	17.78	10.09	12.61	12.63	17.38	24.75	17.08	27.72	17.64	16.89	19.16	17.19
Eu	1.68	2.37	2.09	2.05	2.57	3.17	4.32	2.9	4.4	3.11	2.81	3.33	2.94
Gd	10.49	15.86	7.46	11.27	9.3	11.09	16.1	12.25	20.63	11.99	12.03	13.34	12.72
Tb	1.79	2.35	0.9	1.68	1.16	1.36	2.01	1.57	2.33	1.4	1.44	1.61	1.63
Dy	11.01	13.05	4.66	9.57	5.94	6.7	9.67	7.7	11.54	6.87	7.19	7.94	8.43
Ho	2.48	2.49	0.77	1.91	1.07	1.11	1.62	1.37	1.9	1.1	1.21	1.34	1.51
Er	7.27	7.16	2	5.48	2.92	3.12	4.2	3.54	4.98	3.13	3.16	3.58	4.15
Tm	1.01	1	0.32	0.78	0.4	0.44	0.58	0.5	0.68	0.42	0.42	0.49	0.58
Yb	6.16	6.15	1.95	4.75	2.61	2.88	3.65	2.98	4.18	2.6	2.62	3.07	3.58
Lu	0.9	0.85	0.28	0.68	0.38	0.43	0.51	0.45	0.61	0.38	0.4	0.45	0.52
ASI	1.21	1.09	0.92	1.07	0.49	0.8	0.64	0.6	0.68	0.66	0.63	0.64	0.77
Zr/Hf	38.75	40.35	38.20	39.10	40.90	37.72	38.29	34.85	37.14	38.36	39.09	38.05	38.37
Nb/Ta	17.08	13.83	21.60	17.51	23.44	22.88	22.32	14.73	15.21	16.29	17.44	18.90	18.48
LREE	242.2	456	320.84	339.66	253.23	625.99	770.2	488.26	955.58	616.16	536.55	606.57	526.50
HREE	30.62	33.05	10.88	24.85	14.48	16.04	22.24	18.11	26.22	15.9	16.44	18.49	20.40
LREE/HREE	7.91	13.80	29.49	17.06	17.49	39.03	34.63	26.96	36.44	38.75	32.64	32.28	27.71
REE(tot)	272.81	489.00	331.72	364.51	267.71	642.03	792.44	506.37	981.80	632.06	552.99	625.06	546.89
$(Eu/Eu^*)_N$	0.50	0.42	0.71	0.54	0.69	0.65	0.62	0.59	0.54	0.62	0.57	0.61	0.59
$(La/Yb)_N$	6.33	11.11	26.38	14.60	11.75	35.09	33.89	24.03	40.11	39.21	31.75	30.83	25.96

Av. Pg – Average for Granodiorite only
Av. Sy – Average for Syenite only
Ave - Average for all the granitoid samples*

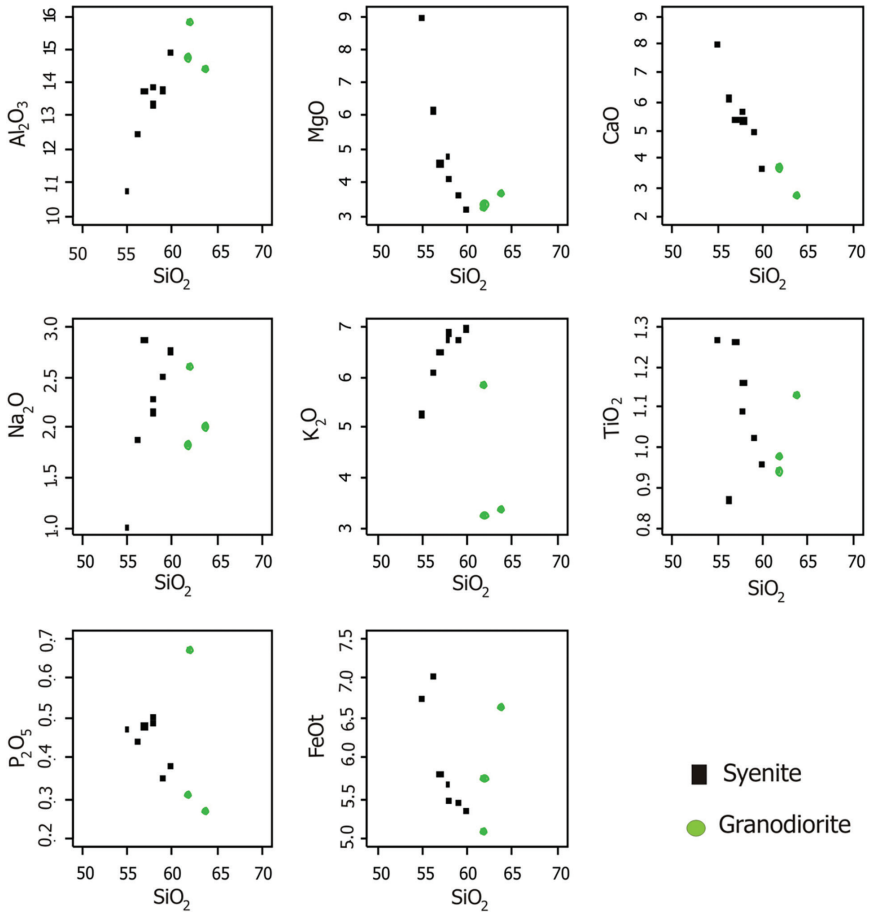


Figure 4: *Harker's plot of SiO_2 vs. other oxides in wt. %.*

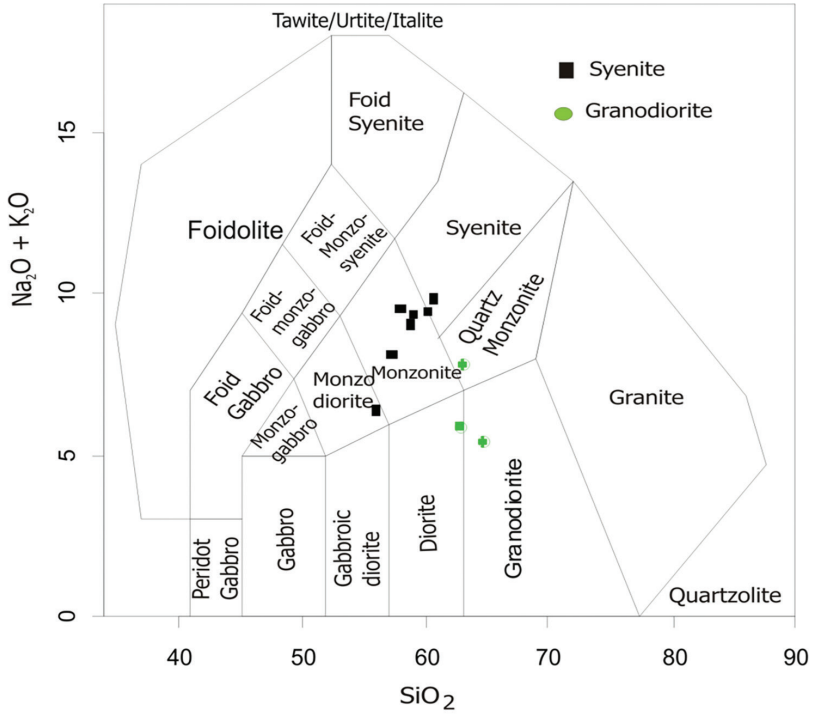
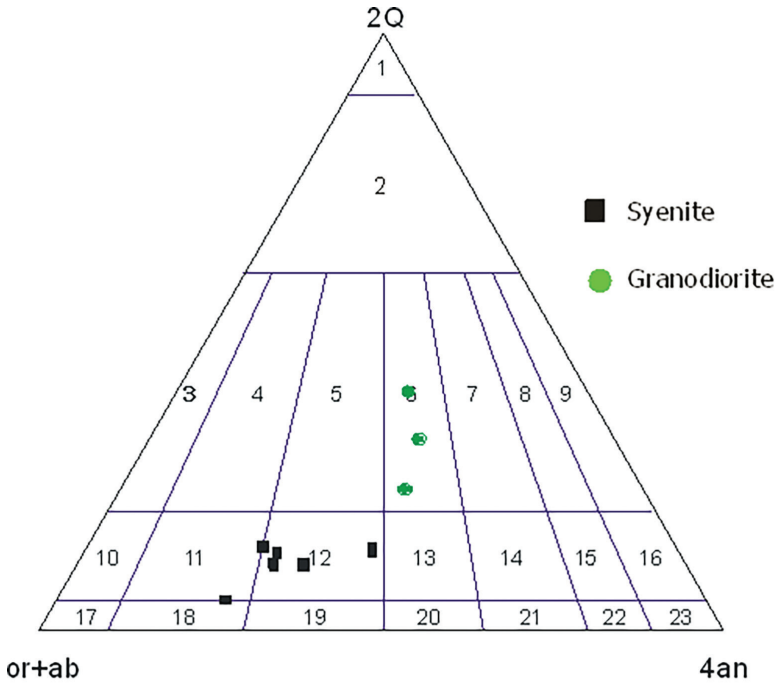


Figure 5: *TAS plot (after Middlemost [19]).*



1. Quartzolite
2. Quartz-rich granitoid
3. Alk-fsp granite
4. Syenogranite
5. Monzogranite
6. Granodiorite
7. Tonalite
8. Tonalgabbro
9. Tonaleucrite
10. Alk-fsp quartz syenite
11. Quartz syenite
12. Quartz monzonite
13. Quartz monzodiorite
14. Quartz diorite
15. Quartz gabbro
16. Quartz eucrite
17. Alkali-feldspar syenite
18. Syenite
19. Monzonite
20. Monzodiorite
21. Diorite
22. Gabbroids
23. Eucritoids

Figure 6: *An adapted QAP diagram using CIPW normative mineralogy [20].*

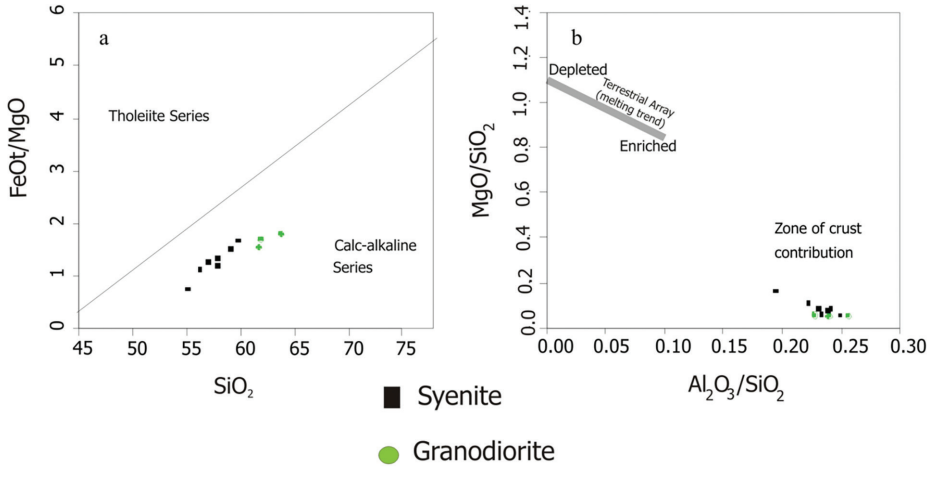


Figure 7: *a) Plot of SiO_2 vs. $FeO_{(tot)}$ [24]. b) Plot of Al_2O_3/SiO_2 vs. MgO/SiO_2 (adapted after Paulick et al. [25]).*

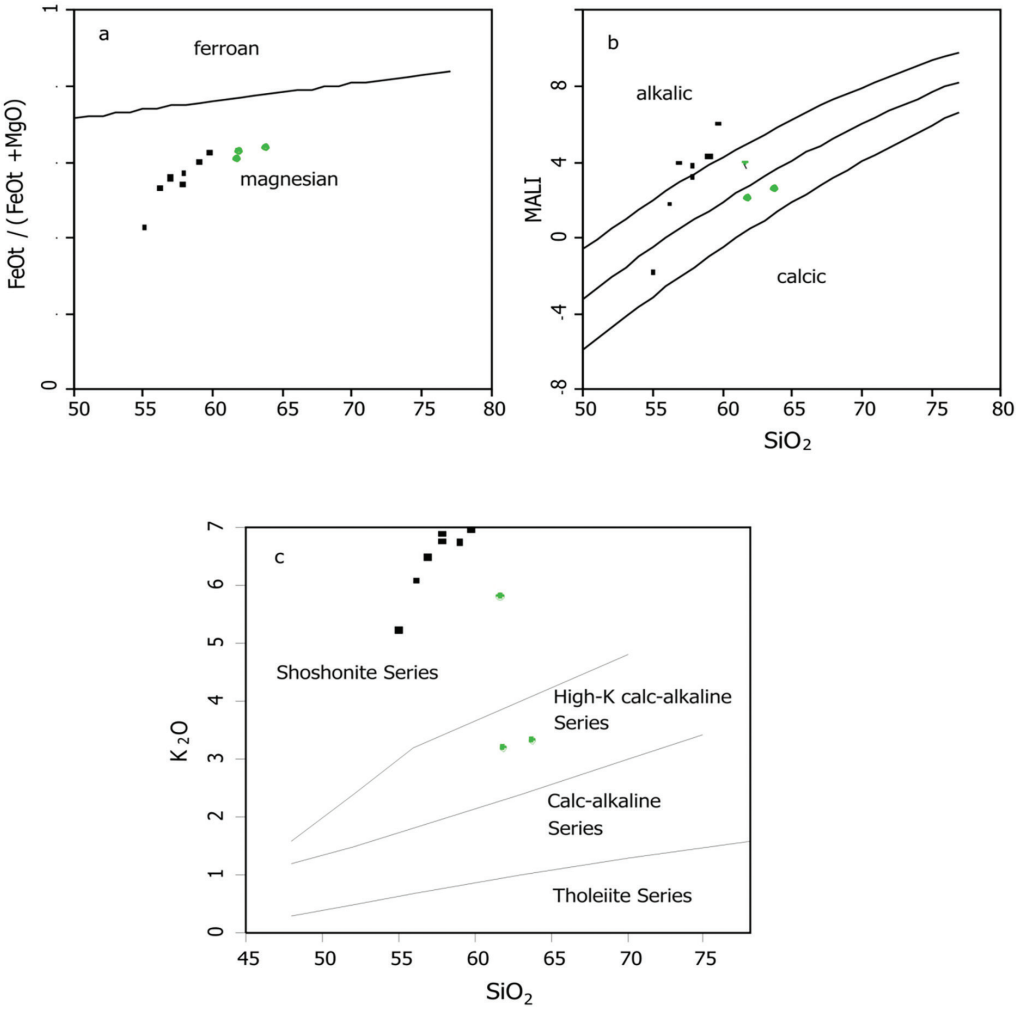


Figure 8: *a) SiO_2 vs. $(FeO+0.9Fe_2O_3)/(FeO+0.9Fe_2O_3+MgO)$ (after Frost & Frost [30]); b) SiO_2 vs. Modified Alkali Lime Index (MALI) (Na_2O+K_2O-CaO) [10], and; c) SiO_2 vs. K_2O (after Peccerillo & Taylor [31]).*

vs. A/NK (Figure 9) as samples from a pluton with metaluminous character.

Samples of the granodiorite plotted in the metaluminous – peraluminous fields. ASI values > 1 were observed for the samples that plotted in the peraluminous field while sample (Pg3) with ASI < 1 plotted in the metaluminous field (Figure 9). Samples of the granodiorite with peraluminous character revealed normative corundum (Table 2) and suggest possible mineralogy consisting of muscovite, cordierite, and presence of aluminosilicate polymorph(s) in addition to those observed from thin section (Table 1).

The syenite body with a metaluminous character suggests that the pyroxene observed from the thin sections is possibly augite occurring in association with hornblende with normative sphene (Tn) (Table 2). The ASI calculation takes into account the presence of apatite [11] while the metaluminous character for the primary magma that formed the syenite pluton, suggesting excess Ca that possibly accounted for the formation of augite (clinopyroxene) and hornblende, agree with the plots of SiO_2 vs. CaO, MgO, $FeO_{(tot)}$ and P_2O_5 where the samples of the granitoid showed a negative correlation (Figure 4) reflecting possible fractionation of apatite, Ca-rich pyroxenes (augite) hornblende.

Concentrations of Zr, Hf, Nb, Ta, Th, U, and REE representing high field strength elements (HFSE) based on ionic potentials were observed

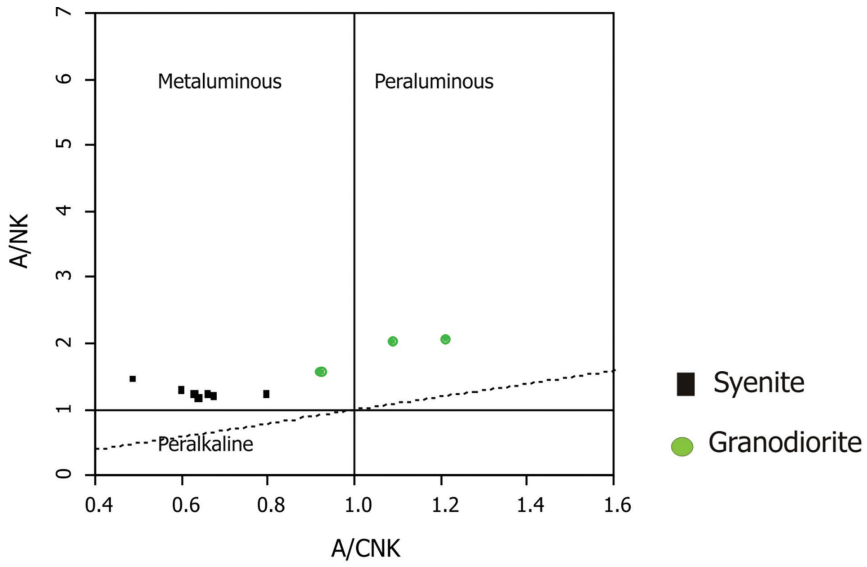


Figure 9: *A/CNK vs. A/NK plot (after Shand [32]).*

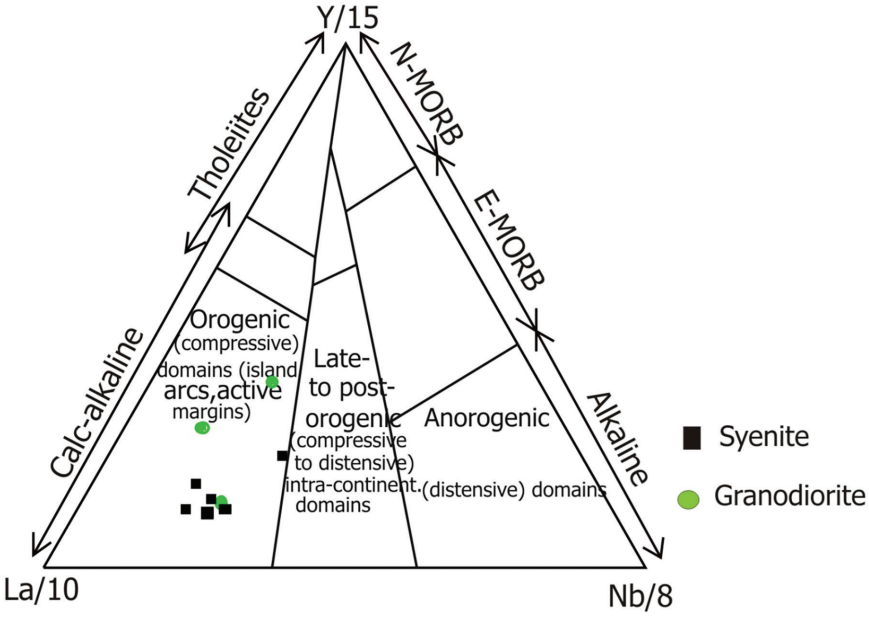


Figure 10: *The trilinear plot of La/10-Y/15-Nb/8 from Cabanis & Lecolle [33] describes geodynamic boundaries for the rocks of the study.*

to be high (Table 3). Zirconium (Zr) concentrations in the granodiorite and syenite ranged from 431.70 ppm to 612.20 ppm and 324.10 ppm to 731.60 ppm, respectively. Hafnium (Hf) concentrations varied similarly. Niobium (Nb) concentrations, observed to be higher in the syenite, gave average values of 19.57 ppm and 36.94 ppm, respectively, for the granodiorite and syenite. Tantalum (Ta) values ranged from 1.00 to 1.20 ppm for the granodiorite and 0.90 to 3.30 ppm for the syenite. The Zr/Hf ratio ranging from 34.85 to 40.90 and Nb/Ta ratio ranging from 0.90 to 3.30 depicted by the syenite samples is representative of the granitoid. The trilinear plot of La-Y-Nb of Cabanis and Lecolle [33] showed that the Okeho granitoids are of calc-alkaline orogenic domain (Figure 10). Trace element plot using HFSE (Ta/Yb vs. Th/

Yb) of Pearce [34] was adapted for this study and shows samples plotted in the volcanic arc domain and supports subduction zone as the environment of emplacement for the granitoids of the study (Figure 11). Geotectonic discrimination diagram for granites adopted for this study showed most samples plotted in the syn-collision granite field in the plot of (Ta+Yb) vs. Rb [12] (Figure 12a) while in the plot of Yb vs. Ta (Figure 12b) samples plotted around the boundaries of syn-collision granite––volcanic arc granite––within plate granite. The geotectonic diagram of Batchelor and Bowden [35] discriminated the granitoids of the study as syn- to post-collision granites (Figure 13). Samples from the granodiorite fell close to the syn-collision field while samples from the syenite fell mainly in the post-collision uplift field.

Trace element enrichment for possible mineralisation

Copper (Cu), lead (Pb), and tin (Sn) mineralisation are commonly associated with granitic ore bodies. The average Cu concentration (Table 3) observed for the granodiorite (Cu, 25.6 ppm) compared well with Taylor and McLennan's [36] Upper Continental Crust (UCC) values (Cu, 25 ppm). In the syenite, an average Cu concentration of 41.07 ppm suggests Cu enrichment. Average UCC values for Pb (17 ppm) and Sn

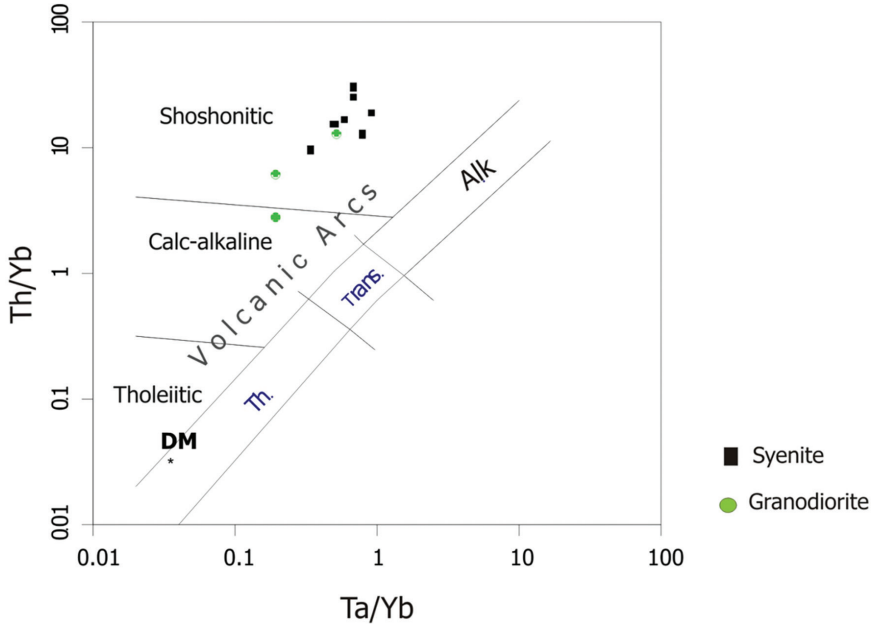


Figure 11: *Ta/Yb vs. Th/Yb diagram characterising magma from volcanic arcs [34].*

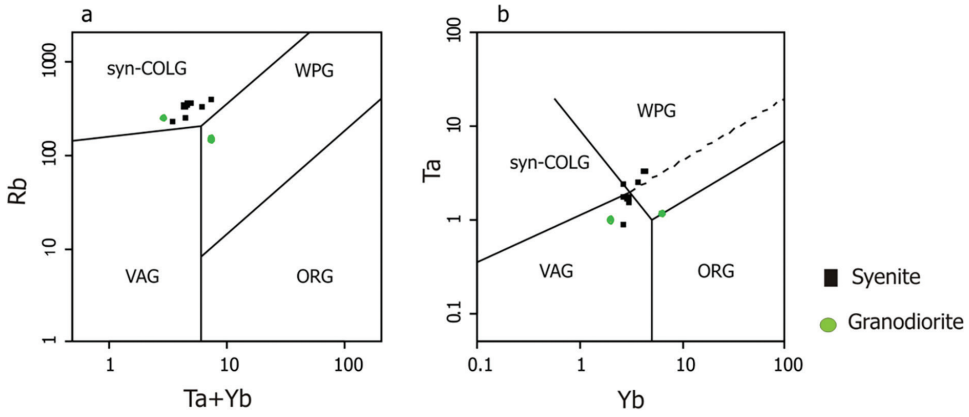


Figure 12: *Granite tectonic discrimination diagram suggests post-orogenic environment for the granitoid rocks of the study [12].*

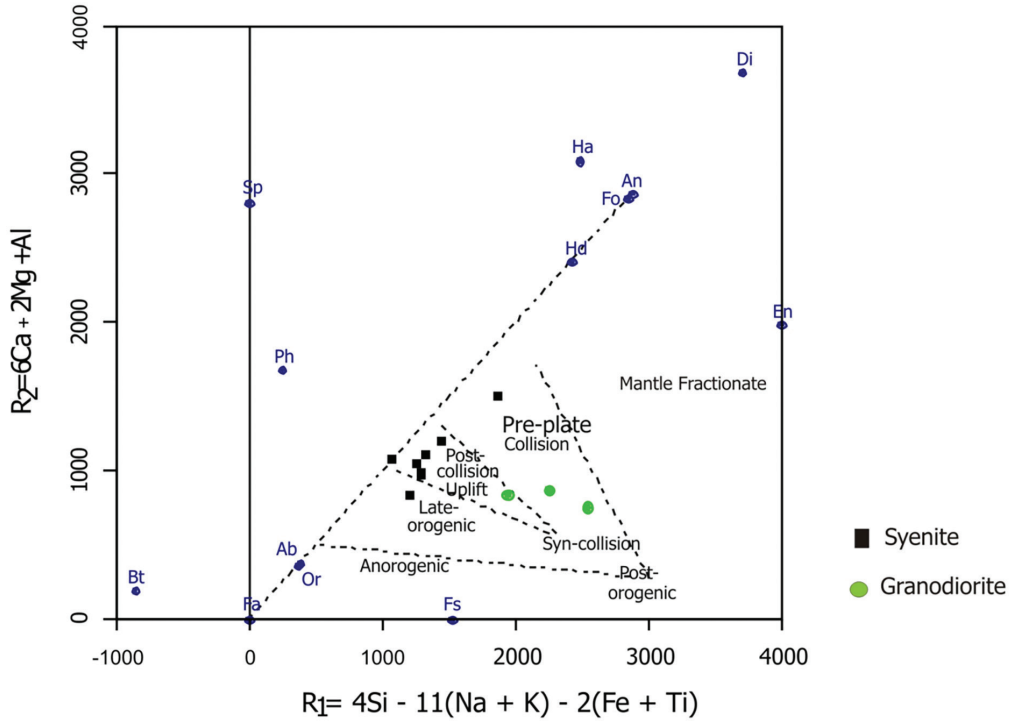


Figure 13: *R1 = (4Si – 11(Na + K) – 2(Fe + Ti) vs. R2 = (6Ca + 2Mg + Al) diagram discriminates geotectonic environment for rocks of the study (after Batchelor & Bowden [35]).*

(5.5 ppm) are higher than Pb (7.30 ppm) and Sn (3.31 ppm) values observed for the granodiorite. Average Pb (20.83 ppm) and Sn (6.86 ppm) values observed for the syenite are higher than UCC average values, respectively. Possible gold (Au) enrichment may be found in the syenite, with an average Au value of 3.50 being almost twice the average Au value (1.80 ppm) reported by [36] for the UCC. Uranium concentrations in both rock types, syenite (6.27 ppm) and granodiorite (5.23 ppm), are observed to be higher than the average UCC uranium value (2.80 ppm).

Rare earth element geochemistry

Average REE values for the granitoids are presented in Table 3. The syenite of the study is enriched in LREEs while the granodiorite is enriched in heavy rare earth elements (HREEs). LREE/HREE ratio shows that the more metaluminous the granitoid is the higher the LREE/HREE ratio. LREE/HREE ratio ranges from 7.91 to 29.49 and 17.49 to 39.03 for the peraluminous granodiorite and the metaluminous syenite, respectively. Sample Pg3 from the granodiorite, which revealed the highest concentrations in K_2O (5.84 wt. %) and Ba (1629 ppm) and plotted in the metaluminous field (Figure 9), showed the highest LREE/HREE (29.49) value for the granodiorite of the study. The average values of total REE concentrations show that the syenite (625.06 ppm) is richer in REE than the granodiorite (364.51 ppm). The average $REE_{(TOT)}$ for the granitoid of the study is 546.89 ppm (Table 3). LREE/REE ratio and $REE_{(TOT)}$ for the granodiorite of the study compared well with the High K calc-alkaline–Shoshonitic granites from Nanling Range, Jiangxi Province, Southern China [37] and peraluminous calc-alkaline porphyry granite from Sanjiang Region [38]. Total REE values for the Dingnan and the Wuliting granites from the Nanling Range, Jiangxi Province had $REE_{(TOT)}$ reaching 428.54 ppm and 344.27 ppm respectively. The average LREE/HREE ratio for the study (27.71) exceeded the highest values from Dingnan (15.00) and Wuliting (17.70). The LREE-enriched metaluminous syenite,

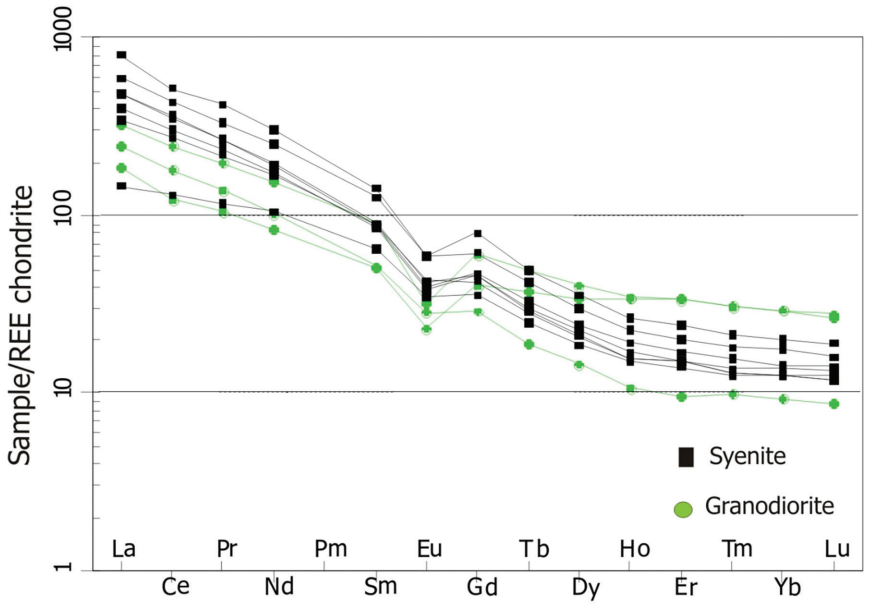


Figure 14: *REE plot normalised using Boynton's [39] chondrite values.*

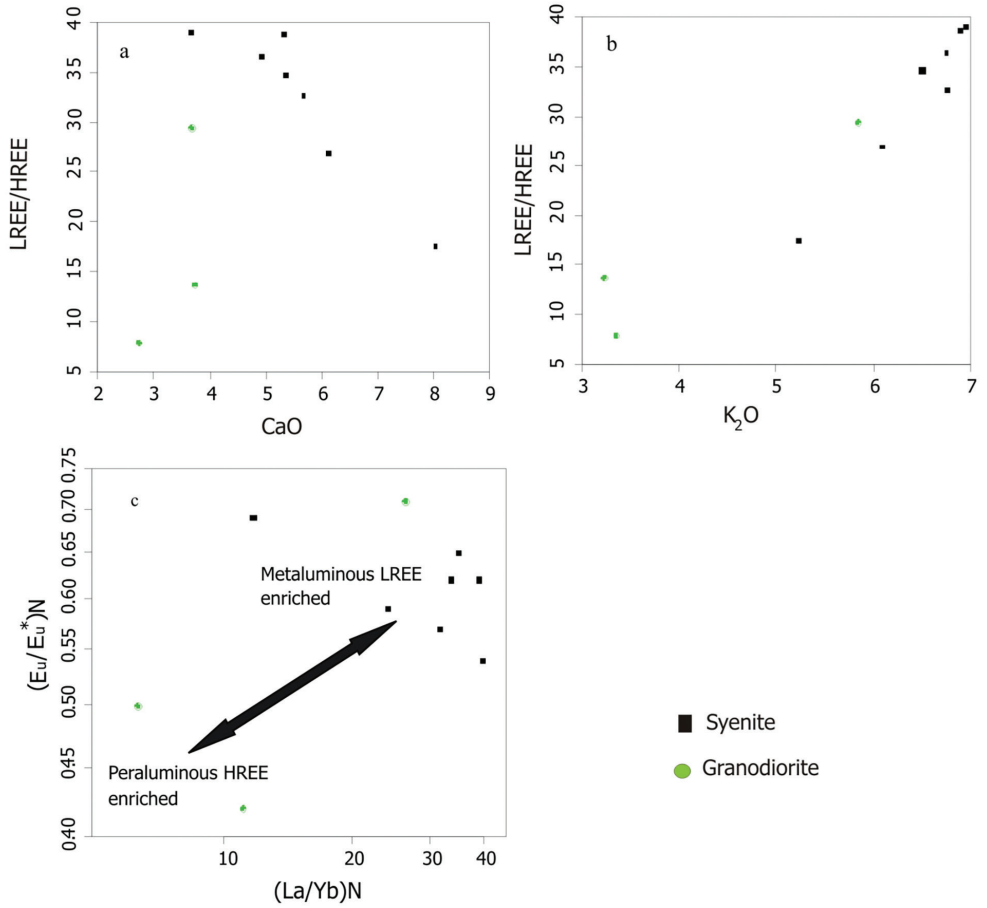


Figure 15: *a) CaO vs. LREE/HREE; b) K_2O vs. LREE/HREE, and; c) (La/Yb)N vs. (Eu/Eu*)N.*

however, showed enrichment in REE concentrations over some of the granite studied from China. The chondrite normalised plot after Boynton [39] (Figure 14) revealed REE enrichment in the granitoids with a negative europium anomaly.

Yang [40] demonstrated that LREE behaviour varies depending on the nature of the magmatic fluid while HREE is fluid-incompatible. The evolution of the granitoids of the study based on the partitioning of LREE in the syenite over HREE in the granodiorite, therefore, suggests varied influence of magma fluxing during cooling, decompression, and degassing. The lithological setting (Figure 1) showing a syenite core with a granodiorite partial ring and the HREE enrichment in the granodiorite may favour an earlier crystallisation of the granodiorite from a melt-rich magma while the syenite core crystallised sometime later from a fluid-rich magma. LREE enrichment can be demonstrated to be related to the fractionation of Ca-rich minerals such as clinopyroxenes and titanite. The plot of CaO vs. LREE/HREE (Figure 15a) showed the syenite, with modal compositions of diopside (Di) and sphene (Tn), having a negative correlation of LREE enrichment, as CaO concentration decreased. Figure 15a revealed an inflection during REE fractionation in the granitoids. With all the samples showing modal orthoclase, with the syenite having higher amounts, the plot of K_2O vs. LREE/HREE (Figure 15b) suggests LREE enrichment with increased fractionation of K-feldspar. $(La/Yb)_N$ vs. $(Eu/Eu^*)_N$ plot discriminated the LREE enriched samples with metaluminous character from the HREE enriched peraluminous samples (Figure 15c).

Conclusion

Granitoids from Okeho in Southwestern Nigeria showed varied mineralogical compositions. The syenite core is richer in hornblende and feldspar but contains less quartz and biotite. The syenite is characterised by the presence of pyroxene and garnet while the granodiorite is depleted in these minerals. The granitoids are peraluminous to metaluminous and possibly derived from a magma derivative having a High-K calc-alkaline to shoshonitic character. The whole rock chemistry suggests that they were emplaced in an orogenic setting of syn-collision to the post-collision environment. The SiO_2 vs. $(FeO+0.9Fe_2O_3)/(FeO+0.9Fe_2O_3+MgO)$ plot of Frost and Frost [30] discriminated the granitoids as magnesian granitoids while normative mineralogy contrasted the granitoid as a metaluminous syenite with normative diopside (Di) and sphene (Tn) from the peraluminous granodiorite with normative corundum (C) and rutile (Ru).

This study shows that continental volcanic arcs in Precambrian terrains are zones where, amongst other rocks, subduction processes yielded metaluminous granitoids of monzonitic compositions having shonshonitic character that are enriched in LREEs in close association with peraluminous granitoids of granodioritic/dioritic to quartz-monzonitic compositions having a High-K calc-alkaline character, which are in turn richer in HREEs.

REE partitioning observed in the granitoids is probably associated with varying degrees of influence from magma fluxing during cooling, decompression, and degassing. The LREE-rich syenite revealed normative diopside (Di) and sphene (Tn) while the HREE-rich granodiorite revealed normative corundum (C) and rutile (Ru).

References

[1] Handoko, A.D., Sanjaya, E. (2018): Characteristics and genesis of Rare Earth Element (REE) in western Indonesia. *IOP Conference Series: Earth and Environmental Science:* 118, 012077, DOI:10.1088/1755-1315/118/1/012077.

[2] Orris, G.J., Grauch, R.I. (2002): Rare Earth Element Mines, Deposits, and Occurrences. *U.S. Geological Survey Open-File Report*, Tucson, pp. 2–189.

[3] Xie, Y.L., Hou, Z.Q., Goldfarb, R.J., Guo, X., Wang, L. (2016): Rare earth element deposits in China. *Reviews in Economic Geology*, 18, pp. 115–136.

[4] Xu, C., Kynický, J., Smith, M.P., Kopriva, A., Brtnický, M., Urubek, T., Yang, Y., Zhao, Z., He, C., Song, W. (2017): Origin of heavy rare earth mineralization in South China. *Nature Communications,* 8, 14598, DOI:10.1038/ncomms14598.

[5] Krishnamurthy, P. (2020): Rare Metal (RM) and Rare Earth Element (REE) Resources:

World Scenario with Special Reference to India. *Journal of the Geological Society of India,* 95(5), pp. 465–474, DOI:10.1007/s12594-020-1463-7.

[6] Ukeagbu, V.U., Beka, F.T. (2008): Rare-earth elements as source indicators of Pan-African granites from Obudu Plateau, Southeastern Nigeria. *Chinese Journal of Geochemistry*, 27(2), pp. 130–134, DOI:10.1007/s11631-008-0130-2.

[7] Omotunde, V.B., Olatunji, A.S., Abdus-Salam, M.O. (2020): Rare Earth Elements Assessment in the Granitoids of Part of Southwestern Nigeria. *European Journal of Environment and Earth Sciences*, 1(5), pp. 4244–4261, DOI:org/10.24018/ejgeo.2020.1.5.79.

[8] Okunlola, O.A., Ajibola, O.M., Olisa, O.G. (2022): Rare element geochemistry and abundances in syenites and charnockitic rocks of selected locations within Southwestern Nigeria. *Materials and Geoenvironment,* 68(3), pp. 1–10, DOI:10.2478/rmzmag-2021-0018.

[9] Rudnick, R.L., Gao, S. (2003): Composition of the Continental Crust. In: *Treatise on geochemistry*, Vol. 3, Holland, H.D., Turekian, K.K. (eds.). Pergamon: Oxford, pp. 1–64, DOI:10.1016/B0-08-043751-6/03016-4.

[10] White, A.J.R., Chappell, B.W. (1983): Granitoid Types and Their Distribution in the Lachlan Fold Belt, Southeastern Australia. *Geological Society of America Memoirs*, 159, pp. 21–34, DOI.org/10.1130/MEM159-p21.

[11] Frost, B.R., Barnes, C.G., Collins, W.J., Arculus, R.J., Ellis, D.J., Frost, C.D. (2001): A geochemical classification for granitic rocks. *Journal of Petrology,* 42, pp. 2033–2048, DOI: 10.1093/petrology/42.11.2033.

[12] Pearce, J.A., Harris, N.B.W., Tindle, A.G. (1984): Trace element discrimination diagrams for the tectonic interpretation of granitic rocks. *Journal of Petrology*, 25(4), pp. 956–983.

[13] Harris, N.B.W., Pearce, J.A., Tindle, A.G. (1986): Geochemical characteristics of collision-zone magmatism. In: *Collision Tectonics,* Coward, M.P., Ries, A.C. (eds.). Geological Society London Special Publication:UK, 19, pp. 67–81.

[14] Tagami, T., Hasebe, N. (1999): Cordilleran-type orogeny and episodic growth of continents: Insights from the circum-Pacific continental margins. *The Island Arc,* 8(2), pp. 206–217, DOI:10.1046/j.1440-1738.1999.00232.x.

[15] McLemore, V.T. (2014): Rare Earth Elements Deposits in New Mexico. In: *Proceedings of the 48th Annual Forum on the Geology of Industrial Minerals*, Arizona Geological Survey Special Paper #9. Conway, F.M. (ed.). Phoenix: Arizona, pp. 1–16.

[16] Oyawoye, M.O. (1967): The petrology of a potassic syenite and its associated biotite pyroxenite at Shaki, Western Nigeria. *Contributions to Mineralogy and Petrology,* 16, pp. 115–138.

[17] Rahaman, M.A., Tubosun, I.A., Lancelot, J.R. (1991): U-Pb geochronology of potassic syenites from Southwestern Nigeria and the timing of deformational events during the Pan-African Orogeny. *Journal of African Earth Sciences (and the Middle East),* 13(3–4), 387–395, DOI:10.1016/0899-5362(91)90102-5.

[18] Elueze, A.A. (1981): Petrographic studies of metabasic rocks and meta-ultramafites in relation to mineralisation in Nigerian schist belts. *Journal of Mining and Geology*, 18(1), pp. 31–36.

[19] Middlemost, E.A. (1994): Naming materials in the magma/igneous rock system. *Earth-Science Reviews*, 37(3–4), pp. 215–224, DOI: org/10.1016/0012-8252(94)90029-9.

[20] Enrique, P. (2018): Clasificación normativa de las rocas plutónicas saturadas y sobresaturadas en sílice basada en la clasificación modal QAP: El diagrama 2Q-(or+ab)-4an. *Geogaceta*, 63, pp. 95–98.

[21] Lameyre, J., Bowden, P. (1982): Plutonic rock type series: discrimination of various granitoid series and related rocks. *Journal of Volcanological and Geothermal Research*, 14, pp. 169–186.

[22] Cobbings, E.J. (2000): *The Geology and Mapping of Granite Batholiths*. Springer-Verlag: Berlin Heidelberg, 141 p.

[23] Bowden, P., Batchelor, R.A., Chappell, B.W., Didier, J., Lameyre, J. (1984): Petrological geochemical and source criteria for the classification of granitic rocks: a discussion. *Physics of the Earth and Planetary Interiors,* 35, pp. 1–11.

[24] Miyashiro, A. (1974): Volcanic rock series in island arcs and active continental margins. *American Journal of Science*, 274(4), pp. 321–355, DOI: 10.2475/ajs.274.4.321.

[25] Paulick, H., Bach, W., Godard, M., De Hoog, J.C.M., Suhr, G., Harvey, J. (2006): Geochemistry of abyssal peridotites (Mid-Atlantic Ridge, 15°20'N, ODP Leg 209) implications for fluid/rock interaction in slow spreading environments. *Chemical Geology*, 234(3–4), pp. 179–210, DOI: 10.1016/j.chemgeo.2006.04.011.

[26] Barbarin, B. (1999): A Review of the Relationships between Granitoid Types, Their Origins and Their

Geodynamic Environments. *Lithos*, 46, pp. 605–626, DOI: 10.1016/S0024-4937(98)00085-1.

[27] Frost, C.D., Frost, B.R. (2011): On Ferroan (A-type) Granitoids: their Compositional Variability and Modes of Origin. *Journal of Petrology*, 52(1), pp. 39–53.

[28] Bergemann, C., Jung, S., Berndt, J., Stracke, A., Hauff, F. (2014): Generation of magnesian, high-K alkali-calcic granites and granodiorites from amphibolitic continental crust in the Damara orogen, Namibia. *Lithos*, 198–199, pp. 217–233.

[29] Pitcher, W.S. (1987): Granites and yet more granites forty years on. *Geologische Rundschau*, 76, pp. 51–79.

[30] Frost, B.R., Frost, C.D. (2008): A geochemical classification for feldspathic igneous rocks. *Journal of Petrology,* 49, pp. 1955–1969.

[31] Peccerillo, A., Taylor, S.R. (1976): Geochemistry of Eocene calc-alkaline volcanic rocks from the Kastamonu area, Northern Turkey. *Contributions to Mineralogy and Petrology,* 58, pp. 63–81, DOI: 10.1007/BF00384745.

[32] Shand, S.J. (1943): *The Eruptive Rocks*, 2nd ed. John Wiley: New York, 444 p.

[33] Cabanis, B., Lecolle, M. (1989): Le diagramme La/10-Y/15-Nb/8: un outil pour la discrimination des séries volcaniques et la mise en évidence des processus de mélange et/ou de contamination crustale. *Comptes Rendus de l'Academie des Sciences*, Series IIA 309: pp. 2023–2029.

[34] Pearce, J.A. (1982): Trace element characteristics of lavas from destructive plate boundaries. In: *Orogenic Andesites and Related Rocks,* Thorpe, R.S. (ed.). John Wiley and Sons: Chichester, pp. 525–548.

[35] Batchelor, R.A., Bowden, P. (1985): Petrogenetic interpretation of granitoid rock series using multicationic parameters. *Chemical Geology,* 48, pp. 43–55, DOI: 10.1016/00092541(85)900348.

[36] Taylor, S.R., McLennan S.M. (1995): The geochemical evolution of the continental crust. *Review Geophysics,* 33, pp. 241–265.

[37] Ishihara, S., Hua, R., Hoshino, M., Murakami, H. (2008): REE Abundance and REE Minerals in Granitic Rocks in the Nanling Range, Jiangxi Province, Southern China, and Generation of the REE-rich Weathered Crust Deposits. *Resource Geology*, 58(4), pp. 355–372, DOI: 10.1111/j.1751-3928.2008.00070.x.

[38] Tian, M.-J., Li, H., Tamehe, L.S., Xi, Z. (2021): Geochronology and Geochemistry of the Zengudi and Tuobake Granite Porphyries in the Sanjiang Region, SW China: Petrogenesis and Tectonic Significance. *Minerals*, *11,* 404, DOI:10.3390/min11040404.

[39] Boynton, W.V. (1984): Geochemistry of the rare earth elements: Meteorite studies. In: *Rare Earth Element geochemistry,* Henderson, P. (ed.). Elsevier: New York, pp. 63–114. DOI:10.1016/B978-0-444-42148-7.50008-3.

[40] Yang, X. (2019): Using Rare Earth Elements (REE) to decipher the origin of ore fluids associated with granite intrusions. *Minerals*, 9, pp. 426, DOI:10.3390/min11040404:10.3390/min9070426.